JACS JOURNAL OF THE AMERICAN CHEMICAL SOCIETY

Article

Cite This: J. Am. Chem. Soc. 2018, 140, 4712−4720

pubs.acs.org/JACS

Quantitative Profiling of Protein Carbonylations in Ferroptosis by an Aniline-Derived Probe

Ying Chen,[†,‡] Yuan Liu,[†,‡,§] Tong Lan,[†,‡] Wei Qin,[†,§] Yuntao Zhu,[†,‡] Ke Qin,[†,‡] Jinjun Gao,[†,§] Haobo Wang,[†,‡] Xiaomeng Hou,[†,‡] Nan Chen,[†,‡] Jose Pedro Friedmann Angeli,[∥,⊥] Marcus Conrad,[∥] and Chu Wang*[,†,‡,§]

[†]Synthetic and Functional Biomolecules Center, Beijing National Laboratory for Molecular Sciences, Key Laboratory of Bioorganic Chemistry and Molecular Engineering of Ministry of Education, [‡]College of Chemistry and Molecular Engineering, and [§]Peking-Tsinghua Center for Life Sciences, Peking University, Beijing 100871, China

[∥]Institute of Developmental Genetics, Helmholtz Zentrum Munchen, Munchen, Germany

Supporting Information

ABSTRACT: Ferroptosis is a regulated form of necrotic cell death implicated in carcinogenesis and neurodegeneration that is driven by phospholipid peroxidation. Lipid-derived electrophiles (LDEs) generated during this process can covalently modify proteins ("carbonylation") and affect their functions. Here we report the development of a quantitative chemoproteomic method to profile carbonylations in ferroptosis by an aniline-derived probe. Using the method, we established a global portrait of protein carbonylations in ferroptosis with >400 endogenously modified proteins and for the first time, identified >20 residue sites with endogenous LDE modifications in ferroptotic cells. Specifically, we discovered and validated a novel cysteine site of modification on voltage-dependent anion-selective channel protein 2 (VDAC2) that might play an important role in sensitizing LDE signals and mediating ferroptosis. Our results will contribute to the understanding of ferroptotic signaling and pathogenesis and provide potential biomarkers for ferroptosis detection.

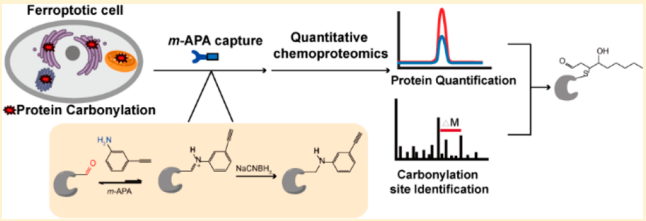

INTRODUCTION

Ferroptosis is a newly annotated form of cell death that has been implicated with diseases such as acute kidney injury, Huntington's disease, cancer, pericentricular leukomalacia, and SECIS-binding protein 2 (SBP2) deficiency syndrome.[1,2] Ferroptosis is morphologically, biochemically, and genetically distinct from other forms of cell death, such as apoptosis, necroptosis, and autophagy.[3−5] Classical hallmarks of ferroptosis include the dependence on intracellular iron and accumulation of phospholipid hydroperoxides.[1,5−7] Two small-molecule ligands have been reported to induce ferroptosis with validated mechanisms. One is erastin which inhibits the cell surface cystine-glutamate antiporter (system x_c^-) resulting in depletion of reduced glutathione and subsequent inactivation of glutathione peroxidase 4 (GPX4).[3] The other is RSL3 that can induce ferroptosis without impacting on GSH level by covalently modifying and inhibiting the activity of GPX4. Due to the unique function of GPX4 in reducing phospholipid hydroperoxides, both erastin and RSL3 are able to trigger the process of lipid peroxidation that culminates with cell death.[5,6] It has been well-known that the process of phospholipid oxidation is able to generate diffusible electrophilic species able to induce specific modifications on proteins that can perturb their activity and function. One major type is often dubbed as "protein carbonylation", which could be derived by Michael addition of a nucleophilic amino acid (cysteine, histidine, or lysine) by an electrophilic α,β-unsaturated aldehyde produced during lipid peroxidation,[8−11] leaving a reactive "carbonyl" group on the target protein. Recent studies have shown that the intracellular concentration of malondialdehyde (MDA), a bona fide lipid-derived electrophile (LDE),[12] is increased when cells succumb to ferroptosis,[1,13] which could potentially result in elevated protein carbonylation and augment ferroptotic signaling. However, the protein targets and specific sites of carbonylation and their roles in ferroptosis remain unexplored.

Several methods have been developed to detect protein carbonylation.[14−16] Cravatt and colleagues reported a competitive activity-based protein profiling (ABPP[17]) strategy to profile targets of LDE modification in cell lysates using a cysteine-reactive iodoacetamide-alkyne (IAyne) probe.[18] Although the method is able to quantify >1000 LDE-sensitive cysteines in proteomes, it suffers from the indirect detection of modifications on only cysteines but not other nucleophilic residues. Bioorthogonal LDE-analogue or precursor probes such as HNE-alkyne have been synthesized and applied to label and enrich targets of protein carbonylation.[19−22] However, these unnatural surrogate probes are not suitable for detecting

Received: February 8, 2018
Published: March 23, 2018

DOI: 10.1021/jacs.8b01462
J. Am. Chem. Soc. 2018, 140, 4712−4720

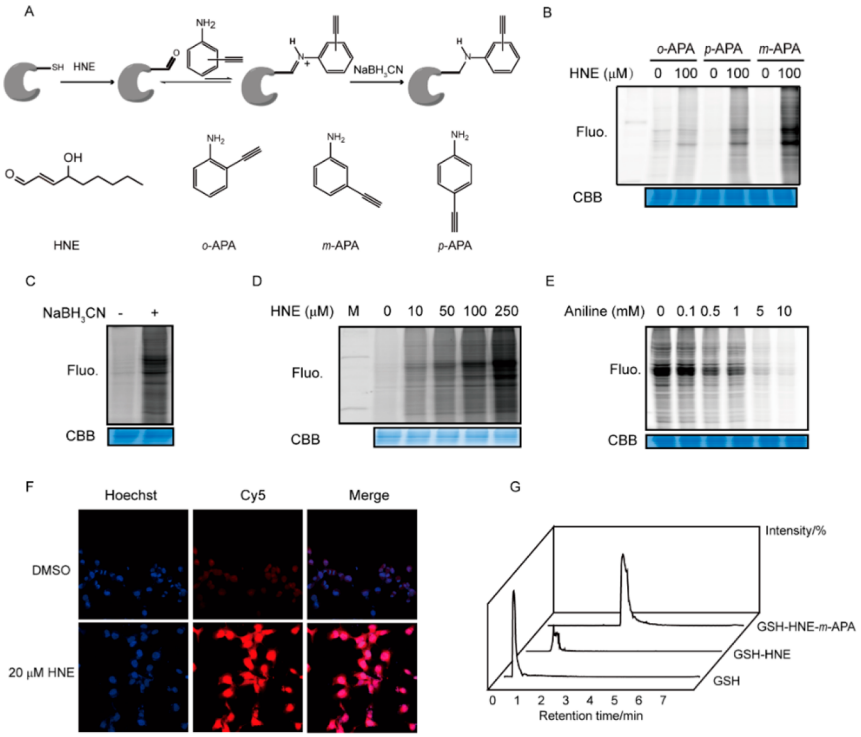

Figure 1. Evaluating the reactivity of aniline probes to detect protein carbonylation in native proteomes. (a) A general scheme of capturing HNE-carbonylated proteins by aniline probes. (b) Comparison of the reactivity of *o*-, *m*-, *p*-APA probes with proteome carbonylations induced by HNE. (c) The reduction by $NaBH_3CN$ is critical in *m*-APA labeling. (d) Detection of concentration-dependent HNE-carbonylations in proteomes by *m*-APA. (e) The labeling of *m*-APA can be effectively competed by free aniline. (f) Imaging of protein carbonylations in HNE-treated cells using *m*-APA by fluorescence confocal microscopy. (g) Confirmation of the adduct of *m*-APA with HNE carbonylated glutathione by LC-MS. Shown are the extracted ion chromatographic traces of GSH, the GSH-HNE adduct, and the final product formed with *m*-APA.

endogenous modification events in cells. Due to its chemical nature, protein carbonylation formed through Michael addition will leave a reactive aldehyde or ketone group on protein targets which enables the selective capture of these modifications with carbonyl-directed ligation probes.

Hydrazide[23−26] and aminooxy probes[27−30] are the most popular choices for capturing protein carbonylations in proteomes. These methods are based on chemoselective imine ligations of aminooxy or hydrazide with aldehyde/ketone to form the covalent oxime or hydrazone adduct, which are widely used in drug delivery, protein labeling and PEGylation.[31−39] Imine formation originally suffered from slow reaction rates which often requires reaction with high concentration of reactants and at acidic conditions, a critical challenge for many biological applications.[32] The limitation was lifted by Dawson and co-workers by their revolutionary discovery of aniline as catalyst to significantly accelerate oxime ligation and hydrazone formation.[40−42] Enhancement of reaction rates follows the mechanism of nucleophilic catalysis where a highly reactive intermediate of protonated aniline Schiff base was quickly formed with aldehyde substrates and a "transimination" reaction then occurs to form the final hydrazone/oxime product. Notably, the aniline Schiff base intermediate can be stabilized by reduction of the imine bond with $NaBH_3CN$, forming the aniline-modified peptide substrates,[41] and this chemistry has also been used in derivatization of aldehyde-containing metabolites and drug intermediates.[43−50] Inspired by these observations, we reasoned that aniline, due to its rapid reaction kinetics and high chemoselectivity with aldehydes, should be applicable as a warhead to react directly with protein targets of carbonylation (Figure 1a).

Herein, we report the development of a unique chemoproteomic platform to profile protein carbonylations using an aniline-based probe. We first validated the approach in the cell lysates modified with 4-hydroxy-2-nonenal (HNE), a well-studied LDE molecule that can cause protein carbonylation, and then applied our method in detecting endogenous target proteins and residue sites of protein carbonylation during ferroptosis.

RESULTS AND DISCUSSION

Evaluating the Reactivity of Aniline Probes to Detect Protein Carbonylation in Native Proteomes. Conveniently, commercially available aminophenylacetylene (APA) compounds with the alkyne group at ortho, para, and meta positions, respectively (Figure 1a), can be readily tested for their efficiency to capture protein carbonylations from cell lysates. Proteomes from nonsmall cell lung cancer H1299 cells were treated with 100 μM of HNE and then labeled with 0.5 mM of each of the APA probes. After reduction with $NaBH_3CN$, the APA-labeled proteins were conjugated with fluorophore-N_3 via copper-catalyzed click chemistry[51] and visualized by in-gel fluorescence. Among the three APA probes, *m*-APA exhibited the best efficiency in reacting with HNE-modified proteomes (Figure 1b). This can be explained by the decreasing electron-withdrawing ability when the alkyne is at the meta position, which gives the strongest nucleophilicity on the aniline warhead. We further found that the optimal pH for *m*-APA labeling is between 5 and 6 (Figure S1a of the Supporting Information, SI), which is consistent with the fact that acidic conditions favor the formation of imine. It is also

DOI: 10.1021/jacs.8b01462
J. Am. Chem. Soc. 2018, 140, 4712−4720

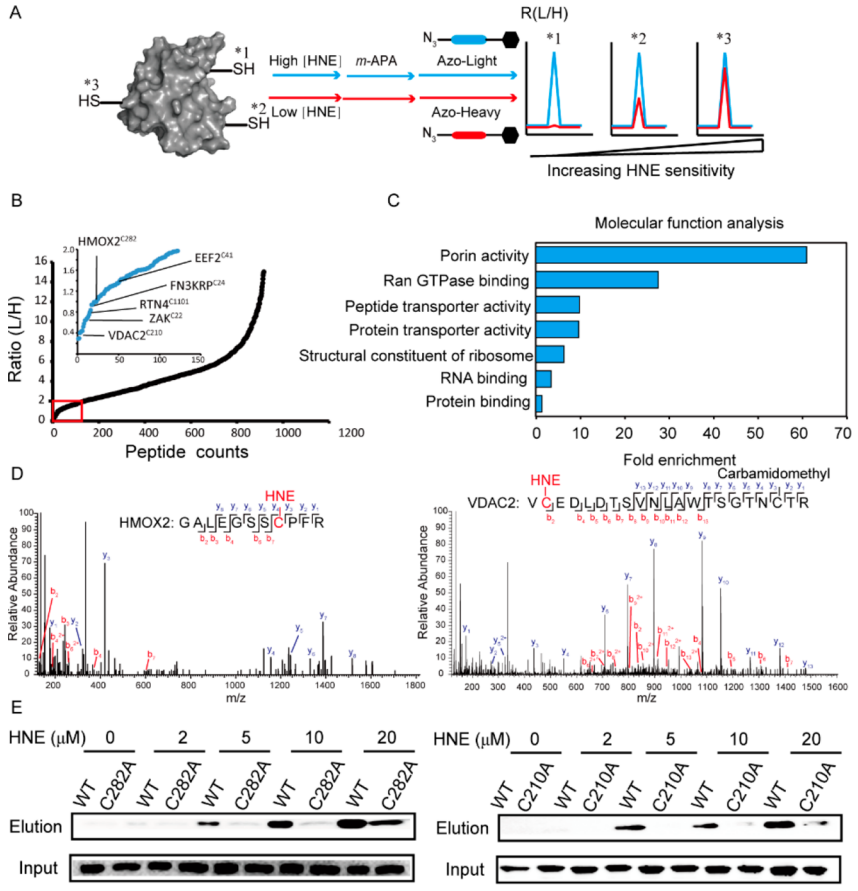

Figure 2. Quantitative profiling of HNE-sensitive sites in proteomes using *m*-APA by isoTOP-ABPP. (a) Scheme of quantifying the sensitivity of HNE modification in proteomes by isoTOP-ABPP. The extent of HNE modifications upon low and high concentrations of HNE treatment was quantified for each site and more saturated labeling (ratio ≈ 1) indicates higher sensitivity toward HNE modification. (b) Distribution of the isoTOP-ABPP ratios for ~1000 cysteines in proteomes upon treatment with 20 and 100 μM HNE. The inlet shows the zoom-in view of the group of HNE-hyper-sensitive cysteines (ratio ≤2.0, red boxed) with representative sites marked (C22 of ZAK, C1001 of RTN4, C282 of HMOX2, and C210 of VDAC2). (c) Gene ontology analysis of proteins harboring HNE-hyper-sensitive cysteines in terms of their molecular functions. (d) MS/MS spectra supporting the HNE modification on C282 of HMOX2 and C210 of VDAC2. (e) *m*-APA selectively labeled carbonylations on C210 of VDAC2 and C282 of HMOX2 in proteomes when cells are treated with increasing concentrations of HNE.

critical to stabilize the imine bond with the reduction step by $NaBH_3CN$ (Figure 1c). The labeling reached saturation at 0.5 mM of *m*-APA and was completed within 60 min (Figures S1b, S2a, and S2b). With these optimized conditions, we showed that *m*-APA was able to monitor protein carbonylations in proteomes induced with various concentrations of HNE (Figure 1d). The labeling could be competed by free aniline (Figure 1e) and was not contaminated by other oxidative forms of cysteine modification, such as protein sulfenylation (Figure S1c). We also treated cells in situ with HNE and demonstrated that *m*-APA can efficiently label carbonylated proteins in fixed cells, enabling direct imaging using confocal microscopy (Figure 1f). In addition, we used the tripeptide glutathione (GSH) as a model to validate the reaction between *m*-APA and carbonylated cysteines. GSH was reacted with 100 μM HNE to form a Michael adduct bearing a free aldehyde and 0.5 mM of *m*-APA was added to continue reaction for 60 min. After reduction of the imine bond with 60 mM $NaBH_3CN$, we successfully detected the GSH-HNE-*m*-APA product (m/z = 563) by UPLC-ESI-MS (Figure 1g). The product was further purified by HPLC and characterized by Fourier Transform Ion Cyclotron Resonance Mass Spectrometry (FTMS) with a correct mass (Figure S26). Lastly, we validated this reaction using a small-molecule substrate, *N*-acetyl-L-cysteine (NAC), and characterized the final adduct by ^{1}H NMR, ^{13}C NMR as well as HRMS (Figure S27, S28, S29, and S30), all of which confirm that *m*-APA is able to capture carbonylated cysteines as predicted.

Identifying Sites of Carbonylation Using a Tandem Orthogonal Proteolysis (TOP)-ABPP Strategy.[52] We continued to combine *m*-APA labeling and TOP-ABPP strategy for identifying HNE modified sites. After proteomes were treated with 100 μM HNE and labeled by *m*-APA, an azide-biotin tag bearing a cleavable azobenzene site ("azo-biotin")[53] was conjugated with the *m*-APA labeled proteins. Following the streptavidin enrichment and on-bead trypsin digestion, an orthogonal round of cleavage was performed by sodium dithionite to release the HNE-modified peptides from the streptavidin beads, which were then analyzed by LC-MS/MS (Figure S3a). We performed three biological replicates and collectively identified >1000 cysteines, 25 histidines and 5 lysines as sites of HNE modifications, which is consistent with previous studies that cysteines are major sites of modifications by HNE through Michael addition[19,54,55] (Figure S3c, Table S1). We also compared the performance of *m*-APA with two other previously reported clickable probes, HZyne and AOyne,[27] side by side. HZyne did not identify any site under the same experimental condition, which is expected from its

DOI: 10.1021/jacs.8b01462
J. Am. Chem. Soc. 2018, 140, 4712−4720

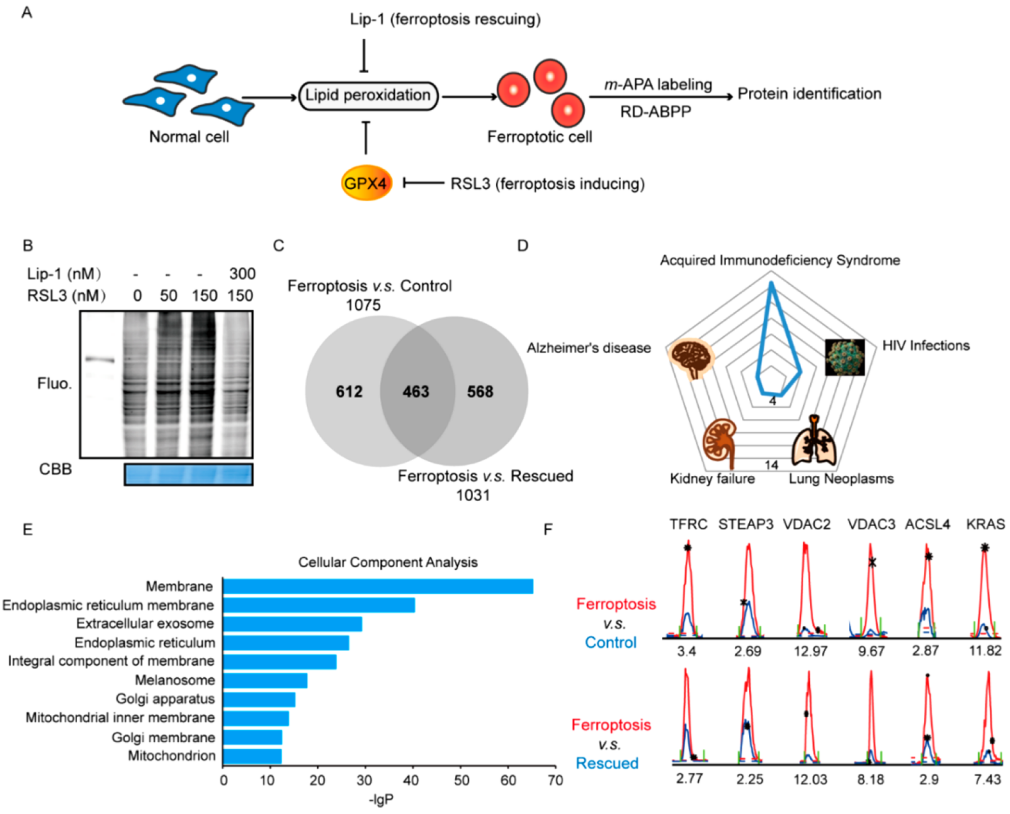

Figure 3. Quantifying endogenous protein carbonylations in ferroptosis using *m*-APA with RD-ABPP. (a) Lipid peroxidation plays an important role in mediating ferroptosis as RSL3 can induce ferroptosis by inhibiting GPX4, a critical detoxifying enzyme for lipid peroxidation and Lip-1 can rescue cells from ferroptosis by scavenging products from lipid peroxidation. (b) Detection of protein carbonylations in ferroptotic HT1080 cells after induced with 0, 50, 150 nM RSL3 and/or rescued by 300 nM Lip-1. (c) A venn diagram showing the number of carbonylated proteins identified in ferroptotic cells vs control or rescued cells. (d) Disease analysis of carbonylated proteins in ferroptosis. (e) Cellular component analysis of carbonylated proteins in ferroptosis. (f) Raw chromatographic peaks of selected proteins quantified with carbonylation in ferroptosis. Red and blue are traces of light and heavy dimethylated peptides with protein names and quantified ratios shown above and below, respectively.

weakest labeling as evaluated by in-gel fluorescence (Figure S2a, b). Surprisingly, despite its seemingly better labeling efficiency, AOyne identified only 293 cysteines, 15 histidines and 4 lysines as sites of HNE modifications by TOP-ABPP, which are much less than those identified by *m*-APA (Figure S2a, b and S3b). Further investigation showed that the AOyne-modified peptide adducts were unstable, which were broken at the N−O bond during sample preparation, probably due to a combined condition of high temperature and acidic buffer (Figure S4). These data suggested that *m*-APA is a superior probe for the purpose of labeling protein carbonylations for chemical proteomics analysis by LC-MS/MS. Given cysteines were found as the major sites of HNE modifications, we performed secondary structure feature analysis on these HNE-adducted peptides and the results showed a marked preference of HNE for cysteines at coil instead of α-helix and β-sheet (Figure S5a). Interestingly, alignment of local sequences flanking the site of modifications revealed that HNE prefers to modify cysteines when a second cysteine is not available at position X+2 or X−2 (Figure S5b), which is the representative motif (CXXC) of the thioredoxin family. This result suggests that despite their heightened intrinsic reactivity, proteins with a thioredoxin like fold are not preferred targets for HNE modification, which are consistent with our previous finding using the IAyne probe.[18] Among the cysteines identified are several previously reported sites of HNE modification,[18] including C1101 of reticulon-4 (RTN4) and C152 of glyceraldehyde-3-phosphate dehydrogenase (GAPDH) (Figure S6b). We overexpressed these proteins along with their cysteine mutants in HEK-293T cells and immunoblotting showed that, upon HNE treatment, the *m*-APA probe could only capture the wild-type proteins, but not any of the cysteine mutants (Figure S6a, c). These results not only biochemically confirmed these cysteines as the specific sites for HNE modification, but also highlighted the efficiency of the *m*-APA probe in selectively labeling protein carbonylations in complex proteomes.

Quantitatively Ranking the HNE Sensitivity by an Isotopic TOP-ABPP Method ("isoTOP-ABPP").[56] In order to quantitatively rank HNE-sensitive cysteines in proteomes, we next applied the *m*-APA labeling to compare the levels of modification at each site upon treatment with variable concentrations of HNE, a strategy which has been used to profile intrinsic chemical reactivity of cysteines in proteomes.[56] Proteomes from H1299 cells were treated with low (20 μM) and high (100 μM) concentrations of HNE independently, labeled with the *m*-APA and conjugated with isotopically labeled heavy and light azo-biotin tags, respectively. The proteomes were combined, enriched, digested by trypsin and cleaved by sodium dithionite before LC-MS/MS analysis. The quantitative ratio (light/heavy) "R" for each HNE-adducted peptide reflects its sensitivity toward HNE modification with lower ratio corresponding to higher HNE sensitivity (i.e., the HNE labeling gets closer to saturation upon treatment with low concentration of HNE) (Figure 2a). We quantified ~1000

DOI: 10.1021/jacs.8b01462
J. Am. Chem. Soc. 2018, 140, 4712−4720

Table 1. Summary of Protein Targets Which Have Potential Links with Ferroptosis in RD-ABPP Results

uniprot #	gene name	ratio (RLS/DMSO)	ratio (+Lip-1/−Lip-1)	potential link with ferroptosis	ref
P02786	TFRC	3.18	2.71	transferrin receptor, with increased expression in ferrotosis-sensitive cells	57
Q658P3	STEAP3	2.44	2.09	function of reducing Fe^{3+} to ferrous iron	2
P45880	VDAC2	12.57	10.71	positive regulator of ferroptosis, direct target of erastin	69
Q9Y277	VDAC3	10.62	7.75	positive regulator of ferroptosis, direct target of erastin	69
O60488	ACSL4	3.12	2.9	regulation of ferroptosis sensitivity by shaping cellular lipid composition	67
P01116	KRAS	11.82	7.56	oncogenic RAS mutant cells sensitive to ferroptosis induced by erastin	68

cysteines with various isoTOP-ABPP ratios and using $R \leq 2$ as the cutoff, we were able to define ∼100 hyper-sensitive cysteines toward HNE modification in proteomes (Figure 2b, Table S2). Analysis of the proteins harboring these HNE-hyper-sensitive cysteines revealed that porin activity is the most significantly enriched molecular function, followed by Ran GTPase binding activity and peptide/protein transporter activity (Figure 2c). We compared the HNE-hyper-sensitive cysteines in our list with those obtained previously using a competitive ABPP method and found that 4 of the top 5 HNE-sensitive cysteines in that list were also identified by our current approach (Figure 2b, Table S3), including C24 of FN3KRP, C22 of ZAK, C1001 of RTN4 and C41 of EEF2.

In addition, we also found several novel HNE-hyper-sensitive cysteines including C210 of voltage-dependent anion-selective channel protein 2 (VDAC2) and C282 of heme oxygenase 2 (HMOX2) (Figure 2d). We overexpressed these two newly identified proteins along with their cysteine mutants in HEK-293T cells and the concentration-dependent HNE treatment of living cells showed that the hyper-sensitive cysteines could be detected at as low as 5 μM of HNE (Figure 2e). Collectively, these results, using HNE as a model compound, demonstrated that *m*-APA is a powerful and efficient probe to capture sites of protein carbonylation both in vitro and in situ for chemical proteomic profiling.

Profiling of the Endogenous Events of Protein Carbonylations in Ferroptosis. Ferroptosis is a newly defined type of cell death that is hallmarked by its dependence on intracellular iron and exacerbated lipid peroxidation. RSL3, a potent inhibitor of GPX4, which is responsible for reducing lipid hydroperoxides to the corresponding alcohols, can potently trigger ferroptosis in HT1080 cells.[57] The cell death can also be efficiently suppressed by liproxstatin-1 (Lip-1), a spiroquinoxalinamine derivative that functions as a catalytic ROS scavenger[7,58,59] (Figure 3a). Consistent with these reports, when we treated HT1080 cells with RSL3 to induce ferroptosis, we observed an increase in lipid ROS which could be blocked by pretreatment of Lip-1 (Figure S7a). We therefore applied the *m*-APA probe in the ferroptotic condition aiming to capture protein carbonylations during this process. Lysates from RSL3-treated and/or Lip-1-treated HT1080 cells were labeled with *m*-APA and conjugated with fluorophore-azide for analysis by in-gel fluorescence. The fluorescence signals increased with the increasing concentrations of RSL3, which supports elevated lipid peroxidation and protein carbonylation in ferroptosis. When Lip-1 was added to rescue cells from ferroptosis, we also observed a concomitant decrease in the *m*-APA labeling signal (Figure 3b), corroborating that the *m*-APA signal detected was indeed derived from endogenously produced LDEs.

In order to quantitatively assess targets of carbonylation in ferroptosis, we implemented a quantitative chemical proteomic platform named "RD-ABPP" that combines reductive dimethylation ("RD") coupled to ABPP.[60,61] Two independent RD-ABPP experiments were designed and performed (Figure S7b). In one experiment, proteomes from control cells and ferroptotic cells were labeled by the *m*-APA probe and the resulting digested peptide samples were subjected to reductive dimethylations by heavy or light formaldehydes, respectively. In the other experiment, proteomes from RSL3-treated cells with and without the ferroptosis inhibitor Lip-1 were labeled with *m*-APA instead. We defined proteins that were quantified in at least two replicates with a light/heavy ratio ≥2 as potential targets and collectively identified 1075 and 1029 carbonylated proteins in each type of the experiments, respectively, with a total number of 461 proteins in common (Figure 3c and Table S4). This data set constitutes, to the best of our knowledge, the first global inventory of carbonylated protein targets modified by endogenous products of lipid peroxidation in ferroptosis.

Gene Ontology (GO) Analysis of Carbonylated Targets in Ferroptosis. GO analysis of the data set revealed that the carbonylated proteins are dominantly localized in the membrane compartments, including Endoplasmic Reticulum (ER) membranes, Golgi apparatus as well as mitochondrial membranes (Figure 3e), which are highly enriched with poly unsaturated fatty acids (PUFAs) that are prone to lipid peroxidation.[62] Interestingly, ER has been shown as a major site of lipid peroxidation during ferroptosis,[7] and it is anticipated that the lipid electrophiles might preferentially target proteins by proximity effect. We also analyzed these carbonylated proteins based on annotations recorded in the DAVID disease database and found that they are highly enriched in diseases such as lung cancer, kidney failure, and Alzheimer's disease (Figure 3d). Most of these diseases have been previously implicated with ferroptosis[1,2,58,63,64] and given that HIV infection can cause dysregulation of glutathione homeostasis[65,66] and induce lipid peroxidation, it is not surprising to find AIDS/HIV infections on the top of the list, too.

Among the list of carbonylated proteins, we found several known targets that have potential links with ferroptosis (Figure 3f, Table 1). For example, ACSL4 has been shown to dictate ferroptosis sensitivity by shaping cellular lipid composition.[67] The oncogenic mutant cell lines of KRAS can be selectively induced into ferroptosis by RSL3.[68] VDAC2/3 were previously identified as the direct targets of erastin, another potent ferroptosis-inducing compound.[69] Notably, our data set also revealed that a couple of vital proteins involved in iron metabolism are carbonylated during ferroptosis including TFRC, a transferrin receptor, and STEAP3, a ferrireductase.[2,57] Normally, Fe^{3+} is imported into cells through TFRC and is then located in the endosome where it is reduced to Fe^{2+} by STEAP3. So it is possible that carbonylation of TFRC and STEAP3 might impede their functions to slow down the overload of Fe^{2+} and reduce its role in catalyzing the ferroptosis process via Fenton reaction. This may act as a negative feedback loop to defend cells from excessive lipid peroxidation as much as possible.

DOI: 10.1021/jacs.8b01462
J. Am. Chem. Soc. 2018, 140, 4712−4720

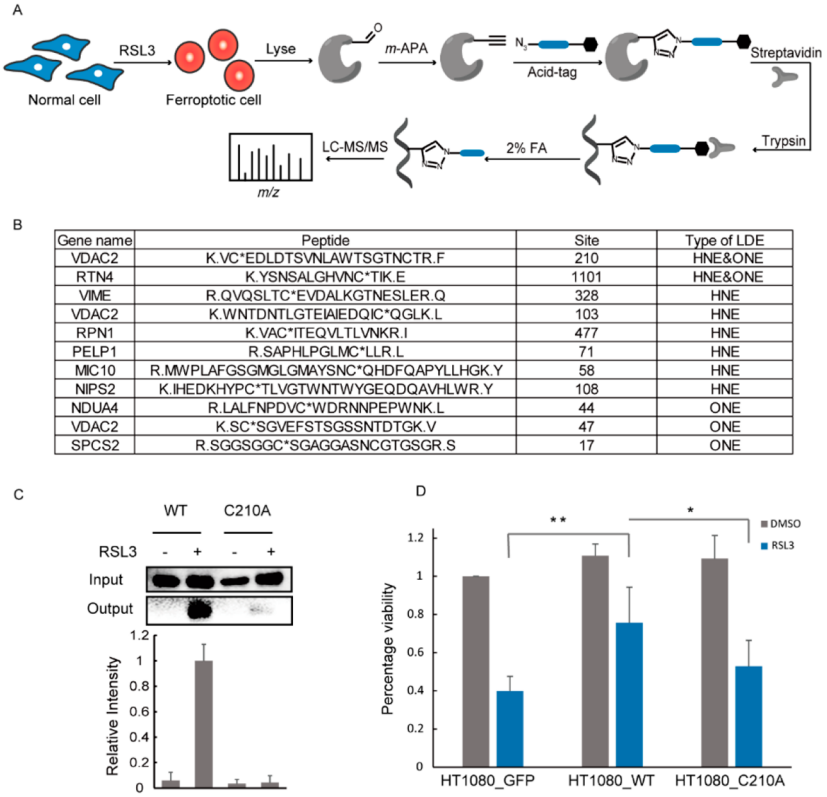

Gene name	Peptide	Site	Type of LDE
VDAC2	K.VC*EDLDTSVNLAWTSGTNCTR.F	210	HNE&ONE
RTN4	K.YSNSALGHVNC*TIK.E	1101	HNE&ONE
VIME	R.QVQSLTC*EVDALKGTNESLER.Q	328	HNE
VDAC2	K.WNTDNTLGTEIAIEDQIC*QGLK.L	103	HNE
RPN1	K.VAC*ITEQVLTLVNKR.I	477	HNE
PELP1	R.SAPHLPGLMC*LLR.L	71	HNE
MIC10	R.MWPLAFGSGMGLGMAYSNC*QHDFQAPYLLHGK.Y	58	HNE
NIPS2	K.IHEDKHYPC*TLVGTWNTWYGEQDQAVHLWR.Y	108	HNE
NDUA4	R.LALFNPDVC*WDRNNPEPWNK.L	44	ONE
VDAC2	K.SC*SGVEFSTSGSSNTDTGK.V	47	ONE
SPCS2	R.SGGSGGC*SGAGGASNCGTGSGR.S	17	ONE

Figure 4. Identification and validation of endogenous LDE modifications in ferroptosis. (a) Scheme of identifying endogenous LDE modified sites in ferroptosis using TOP-ABPP strategy. *m*-APA labeled proteomes were conjugated with an acid cleavable azide-biotin tag and the LDE modified peptides were released by incubation with 2% formic acid for LC-MS/MS analysis. (b) List of selected residue sites with endogenous HNE/ONE modifications in ferroptosis. The full list can be found in Table S5. (c) Validating the endogenous carbonylation on C210 of VDAC2 during ferroptosis as the *m*-APA labeling was lost upon mutation of C210 to alanine. Immunoblotting (top) and signal quantification (bottom) of 6xHis-tagged wildtype VDAC2 and its C210A mutant before ("input") and after ("output") *m*-APA labeling and enrichment. (d) Cell viability test of three HT1080 stable cell lines overexpressing GFP, wildtype VDAC2 and its C210A mutant in the course of ferroptosis induced by RSL3. Values represent means ± SD from six replicate experiments. * $p < 0.05$, ** $p < 0.01$, Student's *t* test.

Identification and Validation of Endogenous Sites of LDE Modifications in Ferroptosis. In addition to identifying carbonylated proteins by products of lipid peroxidation in ferroptosis, it will be highly desired to locate the specific sites with endogenous LDE modifications. Technically, this is a more challenging task because such endogenous modifications are often substoichiometric and unlike protein identification with multiple tryptic peptides, site-specific mapping can only rely on one adducted peptide. After our initial attempt using the azo-benzene enrichment tag failed to identify any endogenously modified sites (data not shown), we turned to an alternative acid cleavable azide-biotin tag which was previously shown to be more robust and efficient to recover probe-labeled peptides in chemoproteomic analysis of protein glycosylations[70−72] (Figure 4a). In the new experimental setting, the peptides were released from the beads through incubation with 2% formic acid and analyzed by LC-MS/MS. We searched the resulting LC-MS/MS data using masses of common LDE adducts (HNE, ACR, ONE, HHE, OHE, and MDA) with multiple filters (see methods), and finally identified 8 endogenous sites of modification by HNE, 11 sites by ACR, and 5 sites by ONE (Figure 4b). This represents, to our best knowledge, the first list of sites of modification by endogenous LDEs in ferroptosis, which will be highly valuable for manifesting the links between lipid peroxidation and ferroptosis.

Among the list of sites of endogenous LDE modifications, VDAC2 attracted our attention because its C210 was identified as hyper-sensitive site toward exogenous HNE modification and the protein was highly enriched by the *m*-APA probe when cells were induced with ferroptosis. More strikingly, C210 was endogenously modified by both HNE and ONE during ferroptosis as unambiguously evidenced by MS/MS spectra (Figure S8). We therefore set out to biochemically validate and functionally characterized the carbonylations on C210 of VDAC2 during cell ferroptosis. We constructed HT1080 cell lines with stable overexpression of wildtype VDAC2 or its C210A mutant. Upon ferroptosis induced by RSL3, the *m*-APA probe could only label the wildtype VDAC2 but not the C210A mutant, confirming carbonylations existing on this specific site (Figure 4c). We next compared the viability of three HT1080 cell lines with stable overexpression of GFP, wildtype VDAC2 and its C210A mutant in the course of ferroptosis induced by RSL3. We found that overexpression of $VDAC2^{WT}$ but not $VDAC2^{C210A}$ could partially protect cells from ferroptosis (Figure 4d), possibly by quenching the LDE signals during this process. These data suggested that endogenous LDE modifications on C210 of VDAC2 are functionally implicated with sensitizing cells to ferroptosis upon RSL3-induced oxidative stress. More thorough biological characterizations remain to be performed to unveil the mechanistic insights linking between these events of LDE modifications and induction of ferroptosis.

DOI: 10.1021/jacs.8b01462
J. Am. Chem. Soc. 2018, 140, 4712−4720

CONCLUSIONS

In summary, we have reported the development and application of an aniline-based probe, *m*-APA, to chemoselectively capture protein carbonylations in proteomes. Using *m*-APA, we directly identified in native proteomes >1000 sites of modification by HNE, a bona fide LDE, and quantitatively ranked their reactivity. We further applied this chemoproteomic strategy to generate, to our best knowledge, the first global portrait of protein carbonylations in the course of ferroptosis with >400 endogenously LDE-modified proteins and >20 modified sites. We also biochemically validated a functional cysteine C210 in the mitochondria outer membrane (OMM) anchored channel protein VDAC2 as an endogenous site of LDE modifications which might play an important role in sensitizing LDE signals and mediating cells to ferroptosis. These efforts will facilitate further investigation of the molecular mechanism of ferroptosis and provide a valuable path for biomarker discovery in ferroptosis. Given the high labeling efficiency and chemoselectivity of the *m*-APA probe which is readily available from commercial sources with little cost, we envision that it will be an ideal tool for detecting and capturing protein carbonylations in many other physiological and/or pathological conditions, where ferroptosis, oxidative stress, and lipid peroxidation are centrally involved including neurodegeneration and inflammation.

EXPERIMENTAL SECTION

Testing *m*-APA in a GSH Model. One mM GSH was reacted with 100 μM HNE in Tris-HCl buffer (pH = 7.4) for 1 h at room temperature. The reaction was then adjusted to pH 5.0 and added with 0.5 mM *m*-APA and 60 mM $NaBH_3CN$ for another 1 h. The samples were analyzed on a UPLC-ESI-MS with a peptide BEH C18 column (Waters 300, 1.7 2.1 100 mm) and a quadrupole rods SQ Detector 2 mass spectrometer (Waters Corp.) The ultrapure water and acetonitrile are used as the mobile phase in a 7 min gradient, and the ion chromatographic traces are extracted at m/z 306 for GSH, 462 for GSH-HNE, 563 for GSH-HNE-*m*-APA.

In-Gel Fluorescence Scanning. H1299 cells were grown to 80% confluence, washed three times with PBS and centrifuged at 1000 rpm for 3 min. PBS supernatant were removed and the cell pallets were stored at −80 °C. The cell pallets were lysed by sonication in ice-cold PBS containing 0.1% TritonX-100, centrifuged at 100 000*g* for 30 min to remove cell debris, and protein concentrations were determined by BCA protein assay. Proteomes were normalized to 2 mg/mL, incubated with 0, 10, 50, 100, or 250 μM HNE for 1h at room temperature and labeled by 0.5 mM *m*-APA at pH 5.0 for 1 h. Proteomes were precipitated by adding 5 volumetric times of methanol/chloroform (v/v = 4:1) mixture and 3 volumetric times of water, and centrifuged at 10 000*g* for 10 min. The supernatants were discarded, and the proteomes were washed using cold methanol and resuspended in 0.4% (w/v) SDS/PBS. The proteomes were reacted with 1 mM $CuSO_4$, 100 μM TBTA ligand, 100 μM fluorophore-N_3, and 1 mM TCEP for 1 h at room temperature. The proteomes were boiled using sample buffer at 90 °C for 5 min, resolved on 10% SDS-PAGE gels and imaged by ChemiDoc XRS+ (Bio-Rad). The gels were then stained by Coomassie brilliant blue (CBB) to demonstrate equal loading.

To check protein carbonylations in ferroptosis by in-gel fluorescence, HT1080 cells were treated with 0, 50, or 150 nM RSL3, with or without cotreatment with 300 nM of Liproxstatin-1 for 3 h. Cells were collected, lysed by sonication in ice-cold PBS containing 0.5% TritonX-100 and centrifuged at 100 000*g* for 30 min to remove cell debris. The protein concentrations were determined by BCA protein assay and normalized to 2 mg/mL. The procedures of *m*-APA labeling and in-gel fluorescence scanning were conducted as described above.

LSM Confocal Microscopy. HT1080 cells were grown to 70% confluence and incubated with 20 μM HNE for 1 h with serum-free medium. The cells were washed with prewarmed PBS, fixed with PBS containing 4% (v/v) formaldehyde at 37 °C for 15 min, rinsed three times with PBS and permeabilized in PBS containing 0.2% (v/v) TritonX-100 at 37 °C for 10 min. The cells were again rinsed three times with PBS and labeled with 0.5 mM *m*-APA for 1 h. Afterward, the cells were washed three times using PBS with gentle shaking, and clicked with 100 μM BTTAA-$CuSO_4$ complex, 100 μM fluorophore-N_3 and 2.5 mM sodium ascorbate for 15 min at room temperature. Finally, the cells were stained with 25 μg/mL Hoechst 33342 for 10 min to indicate the nucleus region. Images were acquired with Zeiss LSM 700 laser scanning confocal microscope equipped with 63×/1.4 NA oil immersion objective lens.

Identification and Quantification of Exogenously HNE Modified Sites. For identification of HNE modified sites, proteomes treated with 100 μM HNE were labeled by 0.5 mM *m*-APA for 60 min (labeling condition of HZyne and AOyne was same as *m*-APA, except that $NaBH_3CN$ was not needed in the case of AOyne labeling). The proteomes were then reacted with 1 mM $CuSO_4$, 100 μM TBTA ligand, 100 μM biotin-AZO-N_3 (light) tag, and 1 mM TCEP for 1 h. The proteomes were precipitated with methanol/chloroform, resuspended in 1.2% SDS/PBS, and diluted to 0.2% SDS/PBS. The samples were subjected to streptavidin enrichment, and on-bead trypsin digestion according to the published TOP-ABPP protocol.[52] The trypsin digest was separated from the beads through 1400*g* centrifuge, and the beads were washed with 3 × 300 μL PBS, 3 × 300 μL H_2O. The azobenzene cleavage was carried out by incubating the beads with 3 × 75 μL 25 mM sodium dithionite for 1 h at room temperature with gentle rotation.[53] The supernatant was collected, added with 5% formic acid and stored at −20 °C until analysis.

For quantification of HNE modified sites, proteomes were treated with 20 μM and 100 μM HNE separately, labeled with *m*-APA and then clicked with heavy biotin-AZO-N_3 and light biotin-AZO-N_3, respectively. The proteomes were precipitated with methanol/chloroform, combined and resuspended in 1.2% SDS/PBS. The samples were processed by TOP-ABPP protocol as described above.

RD-ABPP for Quantifying Endogenously Carbonylated Proteins in ferroptosis. 8 × 10^6 HT1080 cells were seeded in 15 cm dishes to grow overnight and incubated with DMSO ("control") or 150 nM of RSL3 ("ferroptotic") for 3 h in serum-free medium. The cells were collected, lysed by sonication in ice-cold PBS containing 0.5% TritonX-100 and centrifuged at 100 000*g* for 30 min to remove cell debris. The protein concentrations were determined by BCA protein assay and normalized to 2 mg/mL in volume of 1 mL. Lysates from control or ferroptotic cells were separately labeled by 0.5 mM *m*-APA. Proteomes were precipitated with methanol/chloroform and resuspended in 0.4% SDS/PBS. The samples were added with 1 mM $CuSO_4$, 100 μM TBTA ligand, 100 μM biotin-$(PEG)_2$-N_3, and 1 mM TCEP to react for 1 h. The proteomes were again precipitated with methanol/chloroform, resuspended in 1.2% SDS/PBS, diluted to 0.2% SDS/PBS and subjected to streptavidin enrichment. The enriched proteins were digested by trypsin on-bead in 100 mM TEAB buffer and subjected to reductive dimethylation labeling.[60,73] Briefly, 4% of light or heavy formaldehyde was added to ferroptotic or control proteomes, respectively with 0.6 M sodium cyanoborohydride added simultaneously. The reaction lasted for 1 h at room temperature and sequentially quenched by 1% ammonia and 5% formic acid. Finally, heavy and light labeled peptides were combined, concentrated by speed vacuum, separated by the Fast-seq protocol,[74] and analyzed by LC-MS/MS.

To rescue cells from ferroptosis, HT1080 cells were treated with 150 nM RSL3 together with 300 nM Liproxstatin-1 ("Rescued"). Proteomes from "ferroptotic" and "rescued" cells were subjected to the RD-ABPP protocol as described above.

Identification of Endogenous Sites of LDE Modification in Ferroptosis. For identification of endogenous sites of LDE modification in ferroptotic cells, HT1080 cells were treated with DMSO ("control") or 150 nM of RSL3 ("ferroptotic") as described above in RD-ABPP protocol. The proteomes were labeled by 0.5 mM

DOI: 10.1021/jacs.8b01462
J. Am. Chem. Soc. 2018, 140, 4712−4720

m-APA for 60 min and then reacted with 1 mM $CuSO_4$, 100 μM TBTA ligand, 100 μM biotin-acid-N_3 tag, and 1 mM TCEP for 1 h. The proteomes were precipitated with methanol/chloroform, resuspended in 1.2% SDS/PBS, and diluted to 0.2% SDS/PBS. The samples were subjected to streptavidin enrichment, and on-bead trypsin digestion. The trypsin digest was separated from the beads through 1400*g* centrifugation and the beads were washed with 3 × 300 μL PBS and 3 × 300 μL H_2O. The LDE modified peptides were released by incubating the beads with 2 × 200 μL 2% formic acid for 1h at room temperature with gentle rotation. The beads were washed with 2 × 400 μL 50% acetonitrile/water containing 1% formic acid, and the supernatant was combined, concentrated by speed vacuum, and analyzed by LC-MS/MS.

LC-MS/MS and Data Analysis. Samples were analyzed by LC-MS/MS on Q Exactive series Orbitrap mass spectrometers (Thermo Fisher Scientific) coupled with Easynano-LC. Under the positive-ion mode, full-scan mass spectra were acquired over the m/z range from 350 to 1800 using the Orbitrap mass analyzer with mass resolution of 70 000. MS/MS fragmentation is performed in a data-dependent mode, of which the TOP 20 most intense ions are selected for MS2 analysis a resolution of 17 500 using collision mode of HCD. Other important parameters: isolation window, 2.0 m/z units; default charge, 2+; normalized collision energy, 28%; maximum IT, 50 ms; and dynamic exclusion, 20.0 s.

LC-MS/MS data were analyzed by ProLuCID[75] with static modification of cysteine (+57.0215 Da) and variable oxidation of methionine (+15.9949 Da). For RD-ABPP data, the isotopic modifications (28.0313 and 34.0631 Da for light and heavy labeling respectively) are set as variable modifications on the N-terminal of a peptide and lysines. For TOP-ABPP data, 576.3788 Da is set as variable modification on cysteines. For isoTOP-ABPP data, 576.3788 and 582.3926 Da are set as variable modifications on cysteines.

For HNE, ACR, ONE, OHE, 2-HD, and HHE modifications in ferroptosis, 442.3308, 342.2420, 440.3151, 398.2682, 524.4455, and 400.2838 Da are set as variable modifications on cysteines. The full MS spectra were analyzed to make sure that the mono peak of the isotopic envelope matches the mass of peptide identified by ProLuCID which is critical to distinguish modifications with similar masses, for example, HNE and ONE that differ by only 2 Da. For each modification site we identified, we calculated a confidence score based on MS/MS spectra if there are multiple potential modification sites (C/H/K) in the peptide and normalized the scores to assign probability of modification for each position.[76] For the RD-ABPP results, we calculated fold change and relative *p*-value utilizing one sample *t* test for each protein if there are multiple peptides successfully quantified. The ratios of reductive dimethylation and isoTOP-ABPP were quantified by the CIMAGE software as described previously.[56]

For more details, see the SI.

■ ASSOCIATED CONTENT

Supporting Information

The Supporting Information is available free of charge on the ACS Publications website at DOI: 10.1021/jacs.8b01462.

Supplementary methods and Figures S1−S30 (PDF)
Table S1 (XLSX)
Table S2 (XLSX)
Table S3 (XLSX)
Table S4 (XLSX)
Table S5 (XLSX)
Table S6 (XLSX)

■ AUTHOR INFORMATION

Corresponding Author

*chuwang@pku.edu.cn

ORCID

Chu Wang: 0000-0002-6925-1268

Present Address

⊥Rudolf Virchow Center for Experimental Biomedicine, University of Würzburg, 97080 Würzburg, Germany.

Notes

The authors declare no competing financial interest.

■ ACKNOWLEDGMENTS

We thank Prof. Xing Chen and Ms. Pinou Lv for discussion and help with fluorescence imaging. We thank the Computing Platform of the Center for Life Science for supporting the proteomic data analysis. This work was supported by Ministry of Science and Technology of China (2016YFA0501500), National Science Foundation of China (21472008, 21521003, and 81490741), and a "1000 Talents Plan" Young Investigator Award (C.W.). J.P.F.A. is supported by the Junior Group Leader program from the Rudolf Virchow Center - University of Würzburg.

■ REFERENCES

(1) Yang, W. S.; Stockwell, B. R. *Trends Cell Biol.* **2016**, *26*, 165.
(2) Xie, Y.; Hou, W.; Song, X.; Yu, Y.; Huang, J.; Sun, X.; Kang, R.; Tang, D. *Cell Death Differ.* **2016**, *23*, 369.
(3) Dixon, S. J.; Lemberg, K. M.; Lamprecht, M. R.; Skouta, R.; Zaitsev, E. M.; Gleason, C. E.; Patel, D. N.; Bauer, A. J.; Cantley, A. M.; Yang, W. S.; Morrison, B., 3rd; Stockwell, B. R. *Cell* **2012**, *149*, 1060.
(4) Yang, W. S.; SriRamaratnam, R.; Welsch, M. E.; Shimada, K.; Skouta, R.; Viswanathan, V. S.; Cheah, J. H.; Clemons, P. A.; Shamji, A. F.; Clish, C. B.; Brown, L. M.; Girotti, A. W.; Cornish, V. W.; Schreiber, S. L.; Stockwell, B. R. *Cell* **2014**, *156*, 317.
(5) Dixon, S. J.; Stockwell, B. R. *Nat. Chem. Biol.* **2014**, *10*, 9.
(6) Yang, W. S.; Kim, K. J.; Gaschler, M. M.; Patel, M.; Shchepinov, M. S.; Stockwell, B. R. *Proc. Natl. Acad. Sci. U. S. A.* **2016**, *113*, E4966.
(7) Kagan, V. E.; Mao, G.; Qu, F.; Angeli, J. P. F.; Doll, S.; Croix, C. S.; Dar, H. H.; Liu, B.; Tyurin, V. A.; Ritov, V. B.; Kapralov, A. A.; Amoscato, A. A.; Jiang, J.; Anthonymuthu, T.; Mohammadyani, D.; Yang, Q.; Proneth, B.; Klein-Seetharaman, J.; Watkins, S.; Bahar, I.; Greenberger, J.; Mallampalli, R. K.; Stockwell, B. R.; Tyurina, Y. Y.; Conrad, M.; Bayir, H. *Nat. Chem. Biol.* **2017**, *13*, 81.
(8) Fritz, K. S.; Petersen, D. R. *Chem. Res. Toxicol.* **2011**, *24*, 1411.
(9) Galligan, J. J.; Smathers, R. L.; Fritz, K. S.; Epperson, L. E.; Hunter, L. E.; Petersen, D. R. *Chem. Res. Toxicol.* **2012**, *25*, 1012.
(10) Madian, A. G.; Diaz-Maldonado, N.; Gao, Q.; Regnier, F. E. *J. Proteomics* **2011**, *74*, 2395.
(11) Aldini, G.; Dalle-Donne, I.; Facino, R. M.; Milzani, A.; Carini, M. *Med. Res. Rev.* **2007**, *27*, 817.
(12) Ayala, A.; Munoz, M. F.; Arguelles, S. *Oxid. Med. Cell. Longevity* **2014**, *2014*, 360438.
(13) Xie, Y.; Song, X.; Sun, X.; Huang, J.; Zhong, M.; Lotze, M. T.; Zeh, H. J., 3rd; Kang, R.; Tang, D. *Biochem. Biophys. Res. Commun.* **2016**, *473*, 775.
(14) Chen, Y.; Qin, W.; Wang, C. *Curr. Opin. Chem. Biol.* **2016**, *30*, 37.
(15) Liebler, D. C. *Chem. Res. Toxicol.* **2008**, *21*, 117.
(16) Vasil'ev, Y. V.; Tzeng, S. C.; Huang, L.; Maier, C. S. *Mass Spectrom. Rev.* **2014**, *33*, 157.
(17) Wang, C.; Chen, N. *Huaxue Xuebao* **2015**, *73*, 657.
(18) Wang, C.; Weerapana, E.; Blewett, M. M.; Cravatt, B. F. *Nat. Methods* **2014**, *11*, 79.
(19) Yang, J.; Tallman, K. A.; Porter, N. A.; Liebler, D. C. *Anal. Chem.* **2015**, *87*, 2535.
(20) Vila, A.; Tallman, K. A.; Jacobs, A. T.; Liebler, D. C.; Porter, N. A.; Marnett, L. J. *Chem. Res. Toxicol.* **2008**, *21*, 432.
(21) Kim, H. Y.; Tallman, K. A.; Liebler, D. C.; Porter, N. A. *Mol. Cell. Proteomics* **2009**, *8*, 2080.

DOI: 10.1021/jacs.8b01462
J. Am. Chem. Soc. 2018, 140, 4712−4720

(22) Codreanu, S. G.; Ullery, J. C.; Zhu, J.; Tallman, K. A.; Beavers, W. N.; Porter, N. A.; Marnett, L. J.; Zhang, B.; Liebler, D. C. *Mol. Cell. Proteomics* **2014**, *13*, 849.
(23) Tamarit, J.; de Hoogh, A.; Obis, E.; Alsina, D.; Cabiscol, E.; Ros, J. *J. Proteomics* **2012**, *75*, 3778.
(24) Codreanu, S. G.; Kim, H. Y.; Porter, N. A.; Liebler, D. C. *Methods Mol. Biol.* **2012**, *803*, 77.
(25) Codreanu, S. G.; Zhang, B.; Sobecki, S. M.; Billheimer, D. D.; Liebler, D. C. *Mol. Cell. Proteomics* **2009**, *8*, 670.
(26) Spiess, P. C.; Deng, B.; Hondal, R. J.; Matthews, D. E.; van der Vliet, A. *J. Proteomics* **2011**, *74*, 2380.
(27) Chen, Y.; Cong, Y.; Quan, B.; Lan, T.; Chu, X.; Ye, Z.; Hou, X.; Wang, C. *Redox Biol.* **2017**, *12*, 712.
(28) Chavez, J.; Wu, J.; Han, B.; Chung, W. G.; Maier, C. S. *Anal. Chem.* **2006**, *78*, 6847.
(29) Chavez, J. D.; Wu, J.; Bisson, W.; Maier, C. S. *J. Proteomics* **2011**, *74*, 2417.
(30) Chavez, J.; Chung, W. G.; Miranda, C. L.; Singhal, M.; Stevens, J. F.; Maier, C. S. *Chem. Res. Toxicol.* **2010**, *23*, 37.
(31) Mahmoodi, M. M.; Rashidian, M.; Zhang, Y.; Distefano, M. D. *Curr. Protoc Protein Sci.* **2015**, *79*, 15.4.1.
(32) Zeng, Y.; Ramya, T. N.; Dirksen, A.; Dawson, P. E.; Paulson, J. C. *Nat. Methods* **2009**, *6*, 207.
(33) Nauman, D. A.; Bertozzi, C. R. *Biochim. Biophys. Acta, Gen. Subj.* **2001**, *1568*, 147.
(34) Ulrich, S.; Boturyn, D.; Marra, A.; Renaudet, O.; Dumy, P. *Chem. - Eur. J.* **2014**, *20*, 34.
(35) Agten, S. M.; Dawson, P. E.; Hackeng, T. M. *J. Pept. Sci.* **2016**, *22*, 271.
(36) Venter, P. A.; Dirksen, A.; Thomas, D.; Manchester, M.; Dawson, P. E.; Schneemann, A. *Biomacromolecules* **2011**, *12*, 2293.
(37) Brunel, F. M.; Lewis, J. D.; Destito, G.; Steinmetz, N. F.; Manchester, M.; Stuhlmann, H.; Dawson, P. E. *Nano Lett.* **2010**, *10*, 1093.
(38) Dirksen, A.; Yegneswaran, S.; Dawson, P. E. *Angew. Chem., Int. Ed.* **2010**, *49*, 2023.
(39) Blanco-Canosa, J. B.; Medintz, I. L.; Farrell, D.; Mattoussi, H.; Dawson, P. E. *J. Am. Chem. Soc.* **2010**, *132*, 10027.
(40) Dirksen, A.; Hackeng, T. M.; Dawson, P. E. *Angew. Chem., Int. Ed.* **2006**, *45*, 7581.
(41) Dirksen, A.; Dirksen, S.; Hackeng, T. M.; Dawson, P. E. *J. Am. Chem. Soc.* **2006**, *128*, 15602.
(42) Dirksen, A.; Dawson, P. E. *Bioconjugate Chem.* **2008**, *19*, 2543.
(43) Eggink, M.; Wijtmans, M.; Ekkebus, R.; Lingeman, H.; de Esch, I. J. P.; Kool, J.; Niessen, W. M.; Irth, H. *Anal. Chem.* **2008**, *80*, 9042.
(44) Bawazeer, S.; Muhsen Ali, A.; Alhawiti, A.; Khalaf, A.; Gibson, C.; Tusiimire, J.; Watson, D. G. *Talanta* **2017**, *166*, 75.
(45) Jiang, K.; Zhu, H.; Xiao, C.; Liu, D.; Edmunds, G.; Wen, L.; Ma, C.; Li, J.; Wang, P. G. *Anal. Chim. Acta* **2017**, *962*, 32.
(46) Gangjee, A.; Vidwans, A.; Elzein, E.; McGuire, J. J.; Queener, S. F.; Kisliuk, R. L. *J. Med. Chem.* **2001**, *44*, 1993.
(47) Chehade, K. A.; Andres, D. A.; Morimoto, H.; Spielmann, H. P. *J. Org. Chem.* **2000**, *65*, 3027.
(48) Yang, G.; Tan, Z.; Lu, W.; Guo, J.; Yu, H.; Yu, J.; Sun, C.; Qi, X.; Li, Z.; Guan, F. *J. Proteome Res.* **2015**, *14*, 639.
(49) Xia, B.; Feasley, C. L.; Sachdev, G. P.; Smith, D. F.; Cummings, R. D. *Anal. Biochem.* **2009**, *387*, 162.
(50) Guerry, A.; Bernard, J.; Samain, E.; Fleury, E.; Cottaz, S.; Halila, S. *Bioconjugate Chem.* **2013**, *24*, 544.
(51) Kolb, H. C.; Finn, M. G.; Sharpless, K. B. *Angew. Chem., Int. Ed.* **2001**, *40*, 2004.
(52) Weerapana, E.; Speers, A. E.; Cravatt, B. F. *Nat. Protoc.* **2007**, *2*, 1414.
(53) Qian, Y.; Martell, J.; Pace, N. J.; Ballard, T. E.; Johnson, D. S.; Weerapana, E. *ChemBioChem* **2013**, *14*, 1410.
(54) Doorn, J. A.; Petersen, D. R. *Chem. Res. Toxicol.* **2002**, *15*, 1445.
(55) Schopfer, F. J.; Cipollina, C.; Freeman, B. A. *Chem. Rev.* **2011**, *111*, 5997.
(56) Weerapana, E.; Wang, C.; Simon, G. M.; Richter, F.; Khare, S.; Dillon, M. B.; Bachovchin, D. A.; Mowen, K.; Baker, D.; Cravatt, B. F. *Nature* **2010**, *468*, 790.
(57) Yang, W. S.; Stockwell, B. R. *Chem. Biol.* **2008**, *15*, 234.
(58) Friedmann Angeli, J. P.; Schneider, M.; Proneth, B.; Tyurina, Y. Y.; Tyurin, V. A.; Hammond, V. J.; Herbach, N.; Aichler, M.; Walch, A.; Eggenhofer, E.; Basavarajappa, D.; Radmark, O.; Kobayashi, S.; Seibt, T.; Beck, H.; Neff, F.; Esposito, I.; Wanke, R.; Forster, H.; Yefremova, O.; Heinrichmeyer, M.; Bornkamm, G. W.; Geissler, E. K.; Thomas, S. B.; Stockwell, B. R.; O'Donnell, V. B.; Kagan, V. E.; Schick, J. A.; Conrad, M. *Nat. Cell Biol.* **2014**, *16*, 1180.
(59) Zilka, O.; Shah, R.; Li, B.; Friedmann Angeli, J. P.; Griesser, M.; Conrad, M.; Pratt, D. A. *ACS Cent. Sci.* **2017**, *3*, 232.
(60) Boersema, P. J.; Raijmakers, R.; Lemeer, S.; Mohammed, S.; Heck, A. J. *Nat. Protoc.* **2009**, *4*, 484.
(61) Niphakis, M. J.; Cravatt, B. F. *Annu. Rev. Biochem.* **2014**, *83*, 341.
(62) Fritz, K. S.; Petersen, D. R. *Free Radical Biol. Med.* **2013**, *59*, 85.
(63) Skouta, R.; Dixon, S. J.; Wang, J.; Dunn, D. E.; Orman, M.; Shimada, K.; Rosenberg, P. A.; Lo, D. C.; Weinberg, J. M.; Linkermann, A.; Stockwell, B. R. *J. Am. Chem. Soc.* **2014**, *136*, 4551.
(64) Linkermann, A.; Skouta, R.; Himmerkus, N.; Mulay, S. R.; Dewitz, C.; De Zen, F.; Prokai, A.; Zuchtriegel, G.; Krombach, F.; Welz, P. S.; Weinlich, R.; Vanden Berghe, T.; Vandenabeele, P.; Pasparakis, M.; Bleich, M.; Weinberg, J. M.; Reichel, C. A.; Brasen, J. H.; Kunzendorf, U.; Anders, H. J.; Stockwell, B. R.; Green, D. R.; Krautwald, S. *Proc. Natl. Acad. Sci. U. S. A.* **2014**, *111*, 16836.
(65) Herzenberg, L. A.; De Rosa, S. C.; Dubs, J. G.; Roederer, M.; Anderson, M. T.; Ela, S. W.; Deresinski, S. C.; Herzenberg, L. A. *Proc. Natl. Acad. Sci. U. S. A.* **1997**, *94*, 1967.
(66) Cao, J. Y.; Dixon, S. J. *Cell. Mol. Life Sci.* **2016**, *73*, 2195.
(67) Doll, S.; Proneth, B.; Tyurina, Y. Y.; Panzilius, E.; Kobayashi, S.; Ingold, I.; Irmler, M.; Beckers, J.; Aichler, M.; Walch, A.; Prokisch, H.; Trumbach, D.; Mao, G.; Qu, F.; Bayir, H.; Fullekrug, J.; Scheel, C. H.; Wurst, W.; Schick, J. A.; Kagan, V. E.; Angeli, J. P.; Conrad, M. *Nat. Chem. Biol.* **2017**, *13*, 91.
(68) Dolma, S.; Lessnick, S. L.; Hahn, W. C.; Stockwell, B. R. *Cancer Cell* **2003**, *3*, 285.
(69) Yagoda, N.; von Rechenberg, M.; Zaganjor, E.; Bauer, A. J.; Yang, W. S.; Fridman, D. J.; Wolpaw, A. J.; Smukste, I.; Peltier, J. M.; Boniface, J. J.; Smith, R.; Lessnick, S. L.; Sahasrabudhe, S.; Stockwell, B. R. *Nature* **2007**, *447*, 865.
(70) Szychowski, J.; Mahdavi, A.; Hodas, J. J.; Bagert, J. D.; Ngo, J. T.; Landgraf, P.; Dieterich, D. C.; Schuman, E. M.; Tirrell, D. A. *J. Am. Chem. Soc.* **2010**, *132*, 18351.
(71) Woo, C. M.; Iavarone, A. T.; Spiciarich, D. R.; Palaniappan, K. K.; Bertozzi, C. R. *Nat. Methods* **2015**, *12*, 561.
(72) Qin, W.; Qin, K.; Fan, X.; Peng, L.; Hong, W.; Zhu, Y.; Lv, P.; Du, Y.; Huang, R.; Han, M.; Cheng, B.; Liu, Y.; Zhou, W.; Wang, C.; Chen, X. *Angew. Chem., Int. Ed.* **2018**, *57*, 1817.
(73) Hsu, J. L.; Huang, S. Y.; Chow, N. H.; Chen, S. H. *Anal. Chem.* **2003**, *75*, 6843.
(74) Ding, C.; Jiang, J.; Wei, J.; Liu, W.; Zhang, W.; Liu, M.; Fu, T.; Lu, T.; Song, L.; Ying, W.; Chang, C.; Zhang, Y.; Ma, J.; Wei, L.; Malovannaya, A.; Jia, L.; Zhen, B.; Wang, Y.; He, F.; Qian, X.; Qin, J. *Mol. Cell. Proteomics* **2013**, *12*, 2370.
(75) Xu, T.; Park, S. K.; Venable, J. D.; Wohlschlegel, J. A.; Diedrich, J. K.; Cociorva, D.; Lu, B.; Liao, L.; Hewel, J.; Han, X.; Wong, C. C.; Fonslow, B.; Delahunty, C.; Gao, Y.; Shah, H.; Yates, J. R., 3rd *J. Proteomics* **2015**, *129*, 16.
(76) Kong, A. T.; Leprevost, F. V.; Avtonomov, D. M.; Mellacheruvu, D.; Nesvizhskii, A. I. *Nat. Methods* **2017**, *14*, 513.

DOI: 10.1021/jacs.8b01462
J. Am. Chem. Soc. 2018, 140, 4712−4720